JPEDAV (2010) 31:216–222
DOI: 10.1007/s11669-009-9645-4
1547-7037 ©ASM International

Microstructural Characterization of U-Nb-Zr, U-Mo-Nb, and U-Mo-Ti Alloys via Electron Microscopy

A. Ewh, E. Perez, D.D. Keiser Jr., and Y.H. Sohn

(Submitted April 15, 2009; in revised form November 9, 2009)

Ternary uranium molybdenum alloys are being examined for use as dispersion and monolithic nuclear fuels in research and test reactors. In this study, three such ternary alloys, with compositions U-10Nb-4Zr, U-8Mo-3Nb, and U-7Mo-3Ti in wt.%, were examined using scanning electron microscopy (SEM), x-ray diffraction (XRD), and transmission electron microscopy (TEM) with high angle annular dark field (HAADF) imaging via scanning transmission electron microscopy (STEM). These alloys were homogenized at 950 °C for 96 h and were expected to be single-phase bcc-γ-U. However, upon examination, it was determined that despite homogenization, each of the alloys contained a small volume fraction precipitate phase. Through SEM and XRD, it was confirmed that the matrix retained the bcc-γ-U phase. TEM specimens were prepared using site-specific focused ion beam (FIB) in situ lift out (INLO) technique to include at least one precipitate from each alloy. By electron diffraction, the precipitate phases for the U-10Nb-4Zr, U-8Mo-3Nb, and U-7Mo-3Ti alloys were identified as bcc-(Nb,Zr), bcc-(Mo,Nb), and bcc-(Mo,Ti) solid solutions, respectively. The composition and phase information collected in this study was then used to construct ternary isotherms for each of these alloys at 950 °C.

Keywords experimental phase equilibria, isothermal equilibration, materials characterization, metallic alloys, phase equilibria, ternary phase diagram, transmission electron microscopy

1. Introduction

In 1978, the U.S. Department of Energy launched the Reduced Enrichment for Research and Test Reactors (RERTR) program to convert nuclear research reactors from the use of highly enriched uranium (HEU) to low enriched uranium (LEU) to address safety issues associated with nuclear power.[1,2] In order to develop LEU fuels, many different uranium alloys have been considered, but only a few have proven feasible. In addition to being LEU, there are other criteria to be met in fabricating a high performance fuel (e.g., the alloy must maintain high density and γ-U stability under irradiation). Previous studies have shown that uranium-molybdenum (U-Mo) alloys fulfill the requirements to use LEU in reactors while also preserving the γ-U phase and a relatively high density.[2-7]

While functional, the performance of these fuels is drastically reduced due to interactions between the U-Mo alloy and its Al alloy cladding, which cause the formation of detrimental reaction products. During reactor operation, diffusion occurs producing intermetallic compounds with physical and thermal properties that cause adverse effects on the performance of the materials.[6,8] The reaction layer between the U-Mo and the Al matrix experiences significant volumetric expansion that causes fracturing.[9] Moreover, these compounds have lower thermal conductivities than desired, which results in heat buildup in the fuel particles that in turn accelerates the interdiffusion processes between the U-Mo and the Al alloys.[8,10] The growth and properties of the intermetallic compound layers that develop in the U-Mo/Al system must be controlled in order to improve the functionality and service life of the fuels.

In an attempt to mitigate these detrimental diffusional interactions, the influence of certain alloying additions is being studied. Based on thermodynamic calculations, adding Si in the Al matrix, and the transition metals such as Zr, Ti, V, and Nb to the U-Mo fuel was suggested by Park et al.[11] It is suspected that the most promising candidates for additions to the U-Mo alloys are niobium, titanium, and zirconium.[12] These elements were chosen based on their presumably high solubility within the U-Mo system and their potential ability to suppress the formation of the interaction layer.[3,7,13] However, these additions may result in a faster γ-U decomposition rate; it appears that the decomposition of the metastable γ-U phase has a significant

This paper was presented at the Diffusion in Materials for Energy Technologies Symposium held in San Francisco, CA, USA, February 15-19, 2009. This symposium was co-sponsored by the Alloy Phase Committee of the joint EMPMD/SMD of TMS, the TMS High Temperature Alloys Committee, The TMS/ASM Nuclear Materials Committee, the TMS Solidification Committee, and the ASM-MSCTS Atomic Transport Committee. The symposium was organized by J.C. Lacombe of the University of Nevada, Reno; Y.H. Sohn of the University of Central Florida; C. Campbell of the National Institute of Standards and Technology; A. Lupulescu of the General Electric Company; and J.-C. Zhao, of the Ohio State University.

A. Ewh, E. Perez, and **Y.H. Sohn**, Advanced Materials Processing and Analysis Center, Department of Mechanical, Materials, and Aerospace Engineering, University of Central Florida, Orlando, FL; **D.D. Keiser Jr.,** Idaho National Laboratory, Idaho Falls, ID. Contact e-mail: ysohn@mail.ucf.edu.

effect on the interdiffusion rates.[7,14] Ternary U-Nb-Zr, U-Mo-Nb, and U-Mo-Ti alloys have been developed and are being considered for use as fuels. The first step to understanding the kinetics and mechanisms of diffusion within the U-Nb-Zr/Al, U-Mo-Nb/Al, and U-Mo-Ti/Al systems is to characterize the initial microstructure and phase constituents of the ternary alloys.

2. Experimental Procedure

All alloys examined in this study were cast using high-purity depleted U, Mo, Nb, Zr, and Ti via arc melting. They were melted three times to ensure homogeneity and then drop-cast to form rods of 6.35 mm in diameter. The as-cast U-10Nb-4Zr, U-8Mo-3Nb, and U-7Mo-3Ti alloys were homogenized at 950 °C for 96 h. A disk ¼ in. in diameter and approximately 3 mm in thickness was sectioned from the alloy rods. Each disk was individually epoxy mounted and metallographically polished down to 1 μm using diamond paste for microstructural analysis. All sample preparation was performed under Ar atmosphere in a glove box to prevent hazardous material contamination. Backscatter electron (BSE) micrographs were collected using a Hitachi™ S3500N and a JEOL™ 6400 field emission SEM operated at 20 keV accelerating voltage. X-ray energy dispersive spectroscopy (XEDS) was employed for bulk standardless compositional analysis. For bulk phase constituent identification, x-ray diffraction patterns were acquired for each alloy using a Rigaku™ D-MaxB XRD operating with Cu-Kα radiation at 40 kV and 30 mA. Each initial XRD scan of the polished alloy sections was performed with a 2Θ range from 10° to 130° and a scan rate of 1°/min.

Specimens for TEM were prepared with a focused ion beam (FIB) in situ lift-out (INLO) technique using a FEI™ 200 TEM. Figure 1 presents the steps of the FIB INLO process sequentially. Initially, a Pt layer was deposited onto the selected area of interest, as presented in Fig. 1(a), to protect the surface of the sample from the accelerated Ga^+ ion beam. The high energy Ga^+ beam was utilized to mill material creating a trench on both sides. The edges of the sample were then milled leaving only a small bridge of material so that the sample remained attached to the bulk alloy. Both of these steps are shown in Fig. 1(b). A W omniprobe was then lowered in and Pt was welded to the sample as shown in Fig. 1(c). The partially attached edge of the specimen was then milled completely to release the sample. Figure 1(d) shows the sample milled free after the W omniprobe was attached and ready to be lifted out. The W omniprobe, with the TEM specimen still welded to it, was then lifted away from the stage and lowered toward a slotted copper TEM grid as shown in Fig. 1(e). The sample was then Pt welded to the copper grid. Figure 1(f) presents all the TEM specimens welded onto the same copper grid. Each specimen was thinned further, milled to about 100 nm in thickness in order to obtain electron transparency during TEM analysis. Compositional and microstructural analysis was also performed using a FEI/Tecnai™ F30 300 keV

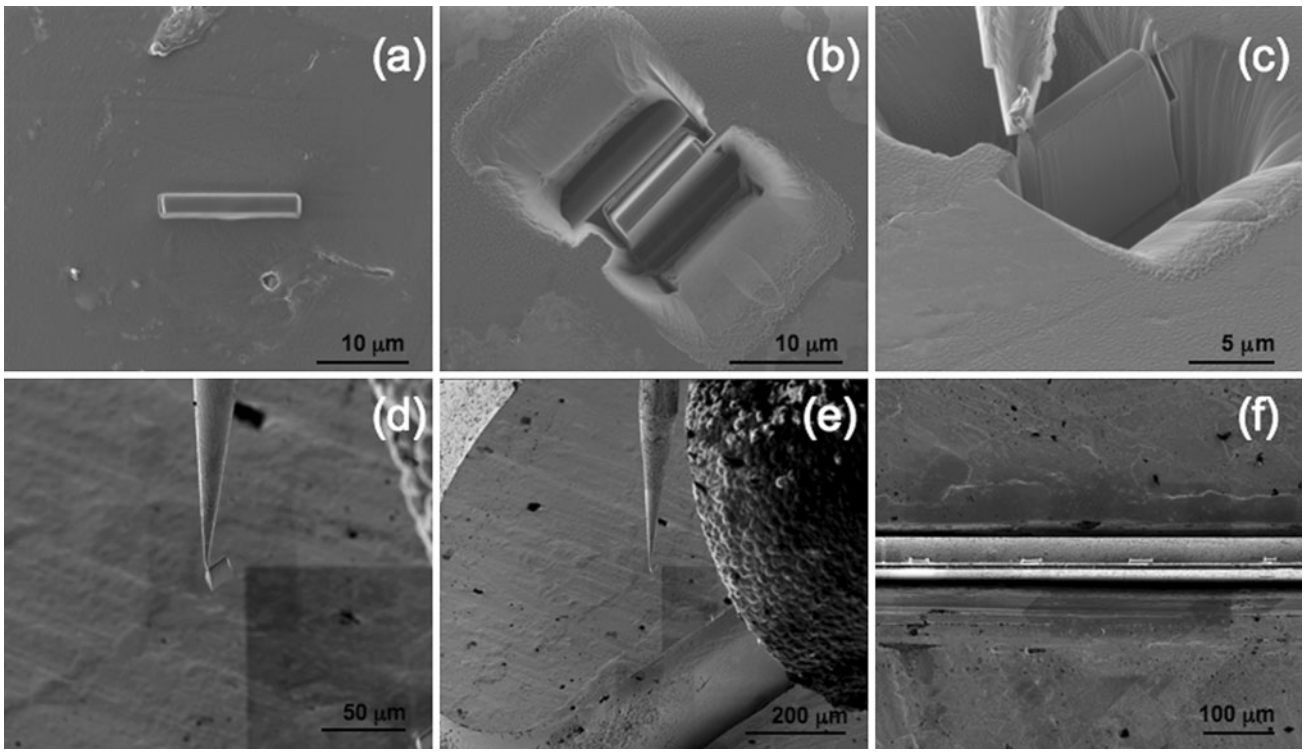

Fig. 1 Focused ion beam (FIB) in situ lift-out (INLO) technique showing the process of TEM specimen preparation

TEM/STEM equipped with a Fischione™ HAADF detector and standardless XEDS. For each specimen, both low and high magnification HAADF STEM images were collected for bulk and detailed analysis. Qualitative XEDS spectra were collected for compositional analysis of distinct features present. Selected area diffraction patterns were collected for the matrix and precipitate phases present and were indexed to identify the phase constituents.

After each of these characterization techniques was performed, the alloy sections were further annealed at 950 °C for an additional 96 h to confirm that the precipitates were near equilibrium. Each of the alloys was separately encapsulated in a quartz capsule and sealed under Ar atmosphere using a high vacuum system. The heat treatment was performed in a Lindberg/Blue™ three-zone tube furnace. Once the alloys were removed from the furnace and rapidly quenched, they were remounted in epoxy and metallographically polished for examination. Another series of BSE images was collected using SEM to confirm that the two-phase microstructure was retained.

3. Results

Initial microstructural characterization was performed using SEM. Figure 2 shows a low magnification BSE image for each of the alloys, which reveals the presence of two phases, i.e., the matrix and a small volume fraction precipitate phase. There are regions of dark contrast as compared to the precipitates, particularly in the U-Mo-Nb alloy. These appear in varying but minor quantities in all of the alloys, are oxide inclusions of casting defects, and are not considered in the remainder of this work. The precipitates appear to be evenly dispersed in all three alloys, are roughly spherical, and are approximately between 2 and

Table 1 Average composition of the bulk ternary alloys

Alloy rod ID	U, wt.%	Mo, wt.%	Nb, wt.%	Ti, wt.%	Zr, wt.%
U-10Nb-4Zr	84.9	…	10.6	…	4.5
U-8Mo-3Nb	88.8	8.3	2.9	…	…
U-7Mo3Ti	88.6	7.5	…	3.9	…

Table 2 Average composition of precipitate phases in ternary alloys measured after the initial anneal at 950 °C for 96 h

Alloy	U, wt.%	Mo, wt.%	Nb, wt.%	Ti, wt.%	Zr, wt.%
U-10Nb-4Zr	14.3 ± 3.9	…	10.5 ± 0.4	…	75.2 ± 4.0
U-8Mo-3Nb	4.1 ± 2.9	60.9 ± 1.8	34.9 ± 1.2	…	…
U-7Mo-3Ti	28.6 ± 0.7	52.8 ± 0.6	…	18.6 ± 0.4	…

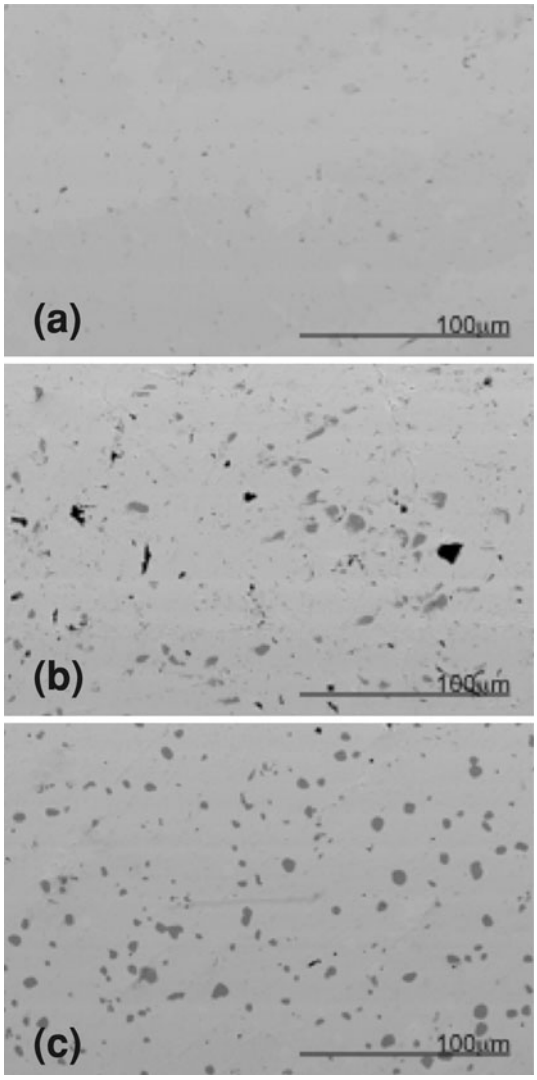

Fig. 2 BSE micrographs of (a) U-10Nb-4Zr, (b) U-8Mo-3Nb, and (c) U-7Mo-3Ti

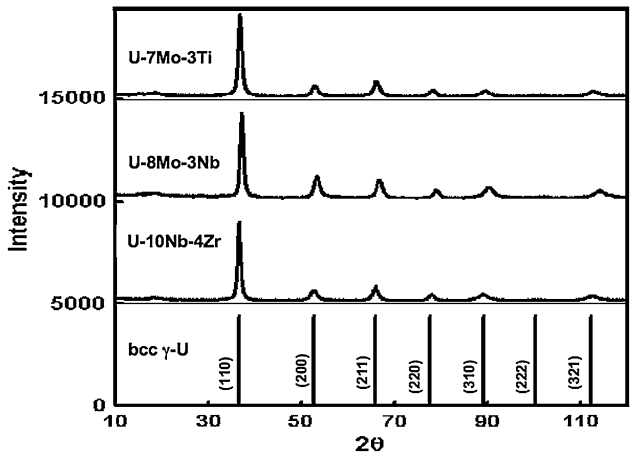

Fig. 3 X-ray diffraction patterns for ternary U-Nb-Zr and U-Mo-X alloys showing bcc-γ-U phase

10 μm in size. The U-7Mo-3Ti alloy seems to have the highest volume fraction while the U-10Nb-4Zr appears to have the lowest. In order to determine compositions, standardless quantitative analysis via EDS was employed. The average compositions for the bulk alloys are presented in Table 1. Average values reported for the bulk alloy analysis agree closely with the targeted nominal compositions of the alloy rods. After collecting overall composition values for the alloy as a whole, compositional data was collected for the precipitate phases separately. The average values for each of the precipitate phases are presented in Table 2. In order to confirm the retention of the bcc-γ-U phase and determine the minor phase constituents of the alloys, XRD patterns were collected for each sample. The indexed patterns are presented in Fig. 3 and show only γ-U with no apparent peaks representing the precipitate phases. The volume fraction of the precipitate phases in these alloys is too low to be detected by XRD.

For detailed analysis of the phase constituents, a TEM specimen was prepared from each of the alloys. HAADF images of each specimen were collected via STEM and are presented in Fig. 4. In the U-8Mo-3Nb and U-7Mo-3Ti images (i.e., Fig. 4b and c), some small remnants of pure U

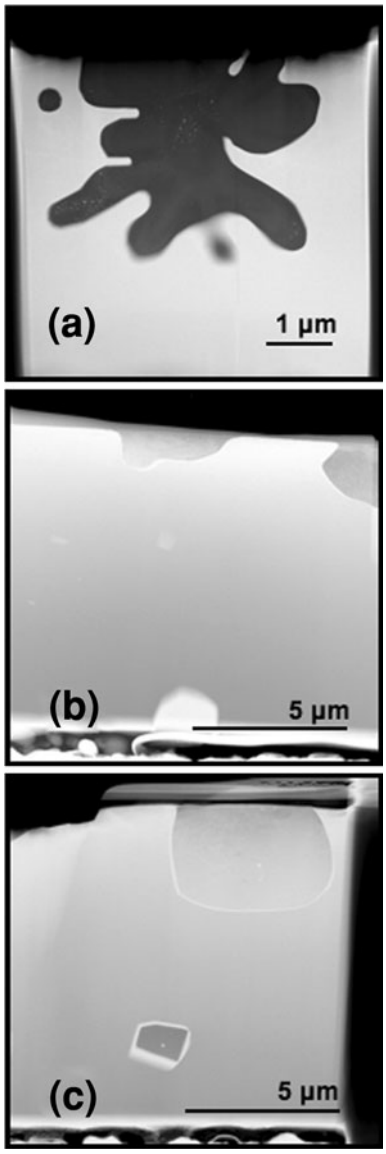

Fig. 4 STEM images of (a) U-10Nb-4Zr, (b) U-8Mo-3Nb, and (c) U-7Mo-3Ti TEM samples

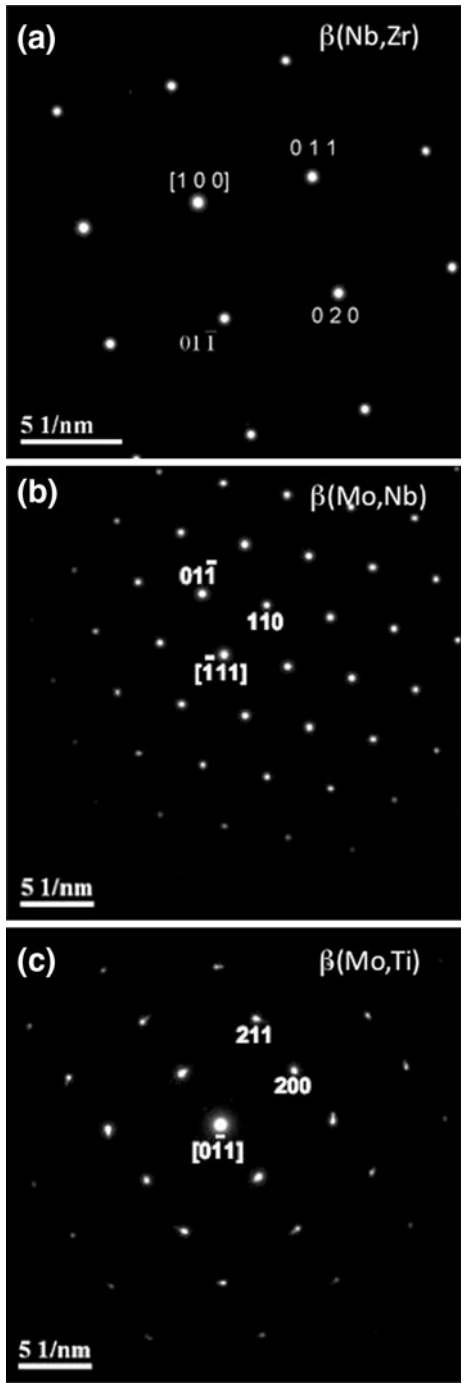

Fig. 5 Electron diffraction patterns for precipitates in (a) U-10Nb-4Zr, (b) U-8Mo-3Nb, and (c) U-7Mo-3Ti

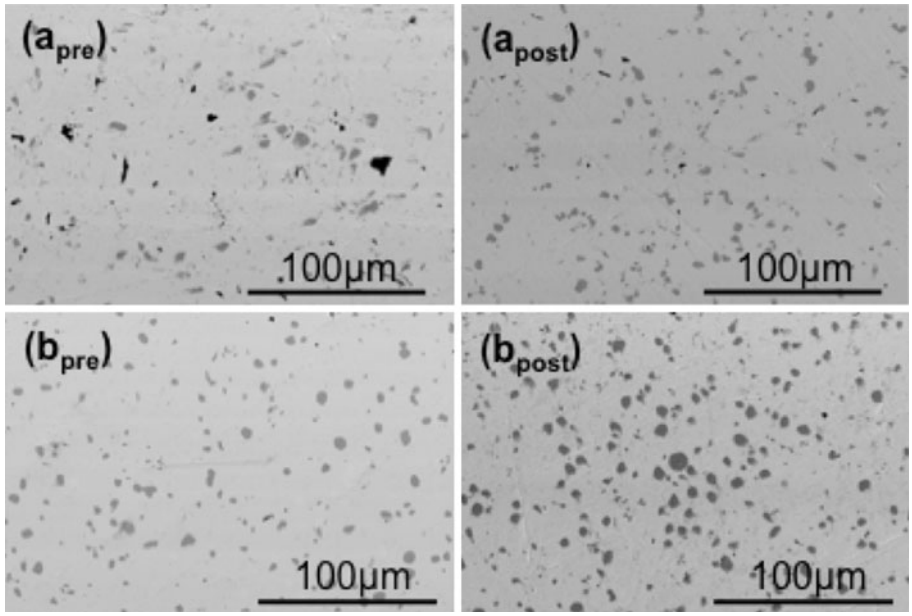

Fig. 6 BSE micrographs of (a) U-8Mo-3Nb and (b) U-7Mo-3Ti pre and post additional 96 h annealing

and pure Ti were visible and identified by XEDS. Electron diffraction patterns were collected to confirm the presence of bcc-γ-U and to identify the precipitate phases. Two different zones were identified and indexed for the matrix and precipitate phases in each alloy. Figure 5 presents representative selected area diffraction patterns gathered for the various precipitate phases. In each case, the precipitate phase indexed to a bcc solid solution phase with relatively low U content. Lattice parameters were calculated for the U-10Nb-4Zr, U-8Mo-3Nb, and U-7Mo-3Ti precipitate phases and have values of a = 3.51, 3.21, and 3.22 Å, respectively.

Upon completion of the TEM analysis, the alloys were further homogenized for an additional 96 h. Micrographs were collected to determine whether or not the precipitate phase was retained after further anneal. Pre and post additional 96 h anneal BSE images are presented in Fig. 6 for comparison. Images for the U-10Nb-4Zr alloy are not shown due to the extremely low area fraction of the precipitates. These micrographs not only show the retention of the precipitate phases, but also indicate area fraction increase. Using ImageJ image analysis software, the area fraction of the precipitate phase in each of these micrographs was calculated. The area fraction determined for the precipitate phase is in the order of 5% and no observable peaks were identified from XRD. The average precipitate area fractions of each alloy before and after the additional anneal are reported in Table 3, and do show an increase after the additional anneal.

Table 3 Area fraction of precipitate phases in U-8Mo-3Nb and U-7Mo-3Ti before and after the additional 96 h anneal at 950 °C

Alloy	Pre, %	Post, %
U-8Mo-3Nb	4.4 ± 1.3	6.6 ± 2.3
U-7Mo-3Ti	5.6 ± 1.9	9.0 ± 1.7

4. Discussion

Initial microstructure characterization shows evenly dispersed precipitates present throughout the alloy section, which indicates that the precipitate formation is a result of the homogenization anneal as opposed to being remnants from casting inhomogeneity. The quantitative EDS data shows that the precipitates are Nb-Zr, Mo-Nb, and Mo-Ti rich. The same precipitate with similar composition were observed by Park et al. in U-Mo-Ti alloys.[11] This suggests that the precipitates represent an equilibrium phase that needs to be identified. Since the casting was performed using pure U, Mo, Nb, Zr, and Ti powders, casting remnants would be in pure elemental form. When the TEM samples were examined, there were features visible that were determined to be pure U and pure Ti in the U-8Mo-3Nb and U-7Mo-3Ti samples, respectively, confirming the former statement regarding casting remnants. In order to verify that the precipitate phases were equilibrium phases and not an intermediate phase that remained due to incomplete homogenization, each alloy section was further annealed at the homogenization temperature for an additional 96 h. The precipitates were still present following the additional annealing and appear to have increased slightly in area fraction, indicating that they are indeed near equilibrium phases.

Since the precipitates are Nb-Zr, Mo-Nb, and Mo-Ti rich, and assuming that the alloys have reached near equilibrium, the binary Nb-Zr,[15] Mo-Nb,[16] and Mo-Ti[17] phase

diagrams were consulted. Each phase diagram shows a bcc solid solution of the two respective components present at the corresponding compositions and temperature of 950 °C. TEM identified the precipitates to be these solid solution phases. Based on all the binary phase diagrams relevant to these systems, however, there should be a large solubility range for any one of the constituents in bcc-γ-U. In fact, one of the suspected advantages of these specific alloying additions compared to other possibilities was their high solubility within γ-U.[7] According to the results of this study, however, the solubility limit of Mo, Nb, Zr, and Ti in γ-U is much lower than expected based on previous literature.

The microstructural and compositional data collected were used to construct schematics of ternary U-Nb-Zr, U-Mo-Nb, and U-Mo-Ti isotherms for 950 °C. Figure 7 presents each of the schematic isotherms constructed. Each of these diagrams illustrates a sharp angle in the phase boundary between single phase γ-U and the two-phase region including the precipitates. This type of boundary would explain the formation of the precipitates observed due to the reduced solubility as compared to the binary systems. The ASM International database of ternary isotherms also shows a few isotherms for these systems at different temperatures with similar construction as those presented here. Further investigations into the reason for the significant decrease in solubility of the ternary system and the separation of the two solid solution phases, i.e., the matrix and precipitate phases, should be considered since one suggested reason for using these particular alloying additions is their high solubility in the U-Mo system. Also, based on these results, these alloying additions may not act effectively as diffusion barriers since they do not remain in

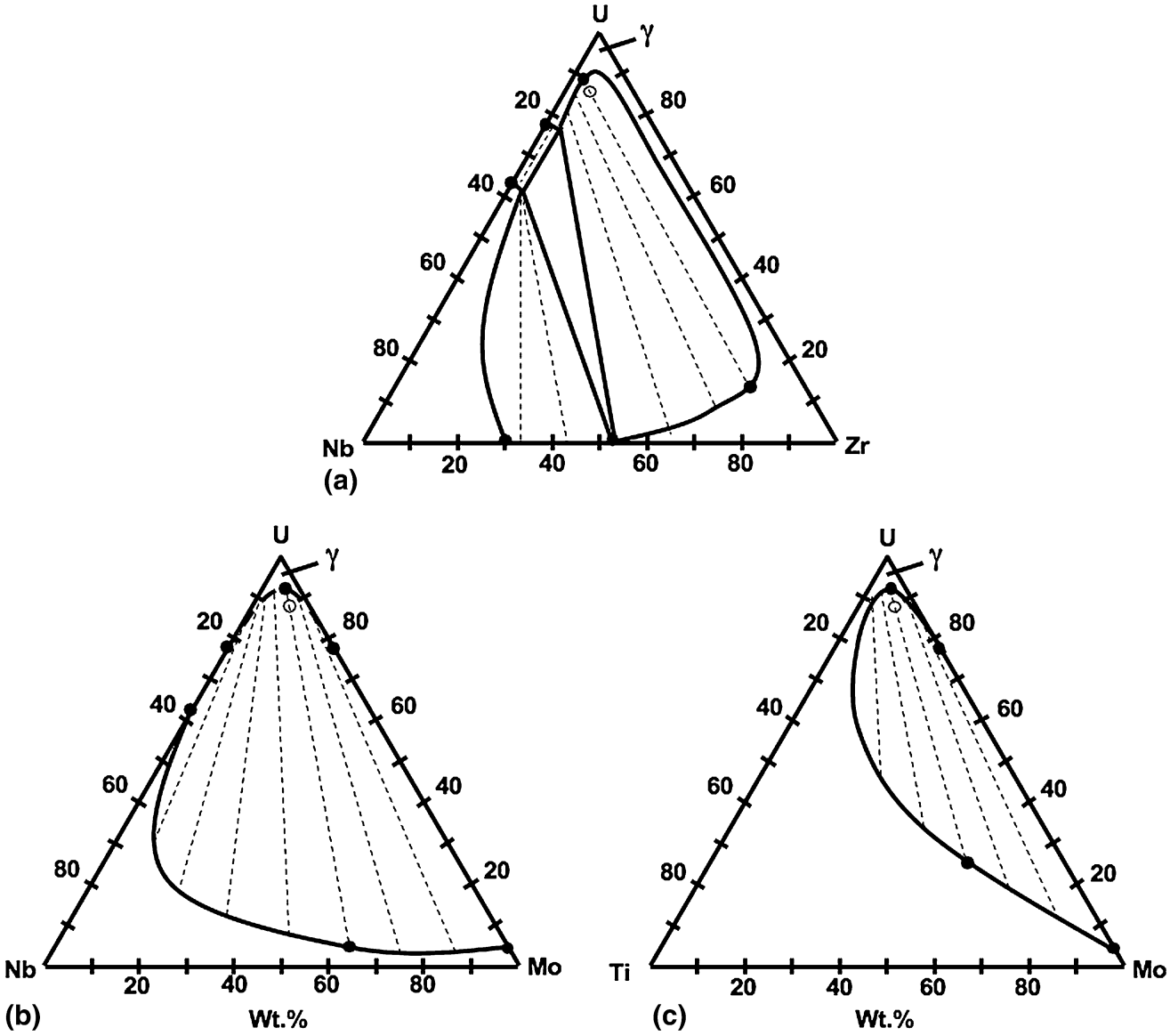

Fig. 7 Estimated ternary isotherms at 950 °C for (a) U-Nb-Zr, (b) U-Mo-Nb, and (c) U-Mo-Ti. *Closed circles* represent phase boundary identified from the equilibrium binary phase diagrams and *open circles* represent the composition of alloys examined in this study

solid solution with the γ-U matrix. A diffusion couple study is currently in progress to determine if this implication is justified.

5. Summary

Currently binary U-Mo alloys are used for fuels in nuclear test reactors. These alloys are functional, but a diffusional interaction between the alloys and the aluminum cladding used in the reactors decreases efficiency and can even cause fuel plate failure. Ternary uranium alloys are being investigated as potential modified fuel alloys. Three such alloys, U-10Nb-4Zr, U-8Mo-3Nb, and U-7Mo-3Ti in wt.%, were examined using SEM, XEDS, XRD, and TEM/STEM to identify phase constituents. Each alloy was found to consist of a bcc-γ-U matrix and a bcc solid solution precipitate phase with low U content. Based on the relevant binary phase diagrams, selected area diffraction patterns and lattice parameter calculations, the precipitate phases were identified for the U-10Nb-4Zr, U-8Mo-3Nb, and U-7Mo-3Ti alloys as bcc-(Nb,Zr), bcc-(Mo,Nb), and bcc-(Mo,Ti) solid solution, respectively. The microstructural and compositional data collected throughout this study were then used to construct ternary isotherms for these three systems at 950 °C.

Acknowledgment

This work was performed with financial support from U.S. Department of Energy (DE-AC07-05ID14517) through Subcontract No. 00062267 administered by Battelle Energy Alliance, LLC and Idaho National Laboratory. Authors would like to thank Prof. John E. Morral at the Ohio State University and Dr. Ursula Kattner at National Institute of Standards and Technology for helpful discussion on phase equilibria.

References

1. M. Meyer, G.L. Hofman, S. Hayes, C. Clark, T. Wiencek, J. Snelgrove, R. Strain, and K.H. Kim, Low-temperature Irradiation Behavior of Uranium-Molybdenum Alloy Dispersion Fuel, *J. Nucl. Mater.*, 2002, **304**, p 221-236
2. H.J. Ryu, Y.S. Han, J.M. Park, S.D. Park, and C.K. Kim, Reaction Layer Growth and Reaction Heat of U-Mo/Al Dispersion Fuels Using Centrifugally Atomized Powders, *J. Nucl. Mater.*, 2003, **321**, p 210-220
3. J.M. Park, H.J. Ryu, S.J. Oh, D.B. Lee, C.K. Kim, and Y.S. Kim, Effects of Si and Zr on the Interdiffusion of U-Mo Alloy and Al, *J. Nucl. Mater.*, 2008, **374**, p 422-430
4. J. Snelgrove, G.L. Hofman, C.L. Trybus, and T.C. Wiencek, *Proceedings of the 18th International Meeting on RERTR*, Seoul, Korea, 1996
5. J. Snelgrove, G.L. Hofman, M.K. Meyer, C.L. Trybus, and T.C. Wiencek, Development of Very-High-Density Low-Enriched-Uranium Fuels, *Nucl. Eng. Des.*, 1997, **178**, p 119-126
6. D.D. Keiser, Jr., C.R. Clark, and M.K. Meyer, Phase Development in Al-rich U-Mo-Al Alloys, *Scripta Mater.*, 2004, **51**, p 893-898
7. G.L. Hofman and M.K. Meyer, Design of High Density Gamma-Phase Uranium Alloys for LEU Dispersion Fuel Applications, *The 1998 International RERTR Conference*, Sao Paulo, Brazil, 1998
8. E. Perez, N. Hotaling, A. Ewh, D.D. Keiser, Jr., and Y.H. Sohn, Growth Kinetics of Intermetallic Phases in U-Mo vs. Al Alloy Diffusion Couples Annealed at 550°C, *Defect Diffus.*, 2007, **266**, p 149-156
9. D.B. Lee, K.H. Kim, and C.K. Kim, Thermal Compatibility Studies of Unirradiated U-Mo Alloys Dispersed in Aluminum, *J. Nucl. Mater.*, 1997, **250**, p 79-82
10. Y.S. Kim, G.L. Hofman, and M.R. Finlay, Argone National Laboratory Intra-Laboratory Memo, Jan. 7, 2004
11. J.M. Park et al., Phase Stability of U-Mo-Ti Alloys and Interdiffusion Behaviours of U-Mo-Ti/Al-Si, *In 2007 International RERTR Meeting*, Prague, Czech Republic, 2007, Paper S15-3
12. Y.S. Kim, G.L. Hofman, Argonne National Laboratory Intra-Laboratory Memo, Feb. 2, 2005
13. M.K. Meyer, G.L. Hofman, T.C. Weincek, S.L. Hayes, and J.L. Snelgrove, Irradiation Behavior of U-Nb-Zr Alloy Dispersed in Aluminum, *J. Nucl. Mater.*, 2001, **299**, p 175-179
14. P.E. Repas, R.H. Goodenow, and R.F. Hehemann, Transformation Characteristics of U-Mo and U-Mo-Ti Alloys, *Trans. ASM*, 1964, **57**, p 150-163
15. H. Okamoto, Phase Diagram Updates, *J. Phase Equilib.*, 1992, **13**, p 577
16. E. Rudy, *Ternary Phase Equilibria in Transition Metal-Boron-Carbon-Silicon Systems, Part V, Compendium of Phase Diagram Data*, Air force Materials Laboratory, Wright-Patterson AFB, OH, Rep. No. AFML-TR-65-2, 1969, p 131-132
17. J.L. Murray, *Phase Diagrams of Binary Titanium Alloys*, ASM, Metals Park, OH, 1987